Heat Transfer Engineering

ISSN: 0145-7632 (Print) 1521-0537 (Online) Journal homepage: https://www.tandfonline.com/loi/uhte20

Modeling and Prediction of Shell-Side Fouling in Shell-and-Tube Heat Exchangers

Emilio Diaz-Bejarano, Francesco Coletti & Sandro Macchietto

To cite this article: Emilio Diaz-Bejarano, Francesco Coletti & Sandro Macchietto (2019) Modeling and Prediction of Shell-Side Fouling in Shell-and-Tube Heat Exchangers, Heat Transfer Engineering, 40:11, 845-861, DOI: 10.1080/01457632.2018.1446814

To link to this article: https://doi.org/10.1080/01457632.2018.1446814

© 2018 Taylor & Francis Group, LLC

Accepted author version posted online: 05 Mar 2018.
Published online: 22 Mar 2018.

Submit your article to this journal

Article views: 2609

View related articles

View Crossmark data

Citing articles: 2 View citing articles

Full Terms & Conditions of access and use can be found at
https://www.tandfonline.com/action/journalInformation?journalCode=uhte20

HEAT TRANSFER ENGINEERING
2019, VOL. 40, NO. 11, 845–861
https://doi.org/10.1080/01457632.2018.1446814

Taylor & Francis
Taylor & Francis Group

Check for updates

Modeling and Prediction of Shell-Side Fouling in Shell-and-Tube Heat Exchangers

Emilio Diaz-Bejarano [a], Francesco Coletti [a,b], and Sandro Macchietto [a,c]

[a]Hexxcell Ltd., Innovation Hub, Imperial College London, London, UK; [b]College of Engineering, Design and Physical Sciences, Brunel University London, Uxbridge, UK; [c]Department of Chemical Engineering, Imperial College London, London, UK

ABSTRACT

Fouling is a challenging, longstanding, and costly problem affecting a variety of heat transfer applications in industry. Mathematical models that aim at capturing and predicting fouling trends in shell-and-tube heat exchangers typically focus on fouling inside the tubes, while fouling on the shell side has generally been neglected. However, fouling deposition on the shell side may be significant in practice, impairing heat transfer, increasing pressure drops, and modifying flow paths. In this paper, a new model formulation is presented that enables capturing fouling on the shell side of shell-and-tube heat exchangers including the effect of occlusion of the shell-side clearances. It is demonstrated by means of an industrial case study in a crude oil refinery application. The model, implemented in an advanced simulation environment, is fitted to plant data. It is shown to capture the complex thermal and hydraulic interactions between fouling growth inside and outside of the tubes, the effect of fouling on the occlusion of the shell-side construction clearances, and to unveil the impact on shell-side flow patterns, heat transfer coefficient, pressure drops, and overall exchanger performance. The model is shown to predict the fouling behavior in a seamless dynamic simulation of both deposition and cleaning operations, with excellent results.

Introduction

Fouling in a variety of heat transfer applications, for example in refinery preheat trains, is a complex, costly, and disruptive problem that has been affecting industry for decades. In recent years, significant progress has been made in the fundamental understanding of the processes leading to fouling [1]–[3] and in the fouling management strategies in industrial practice, involving the regular cleaning of key heat exchangers and/or the use of antifoulants. However, there is still a significant room for improvement, particularly with regards to the design and condition monitoring of heat exchangers. Following a number of critiques of the fouling factor based approach to heat exchanger design [4], [5], a significant effort has been made to develop alternative tools that would more effectively capture, simulate, predict, manage, and, ultimately, mitigate fouling.

Based on experimental measurements, various correlations that describe the thermal resistance given by fouling as a function of process conditions and time have been proposed [6]–[9]. Mathematical models that use such equations [10]–[13] have been developed with the aim of improving existing design and monitoring software tools. One limitation of these models is that they consider deposition of fouling only on the tube-side. Thus their applicability is restricted to cases in which shell-side fouling is negligible.

Traditional design practice recommends allocating the fluid with the highest fouling propensity to the tube side to allow easier and more effective cleaning. However, the shell-side fluid may also be prone to fouling, particularly, in refinery applications, with heavy fractions from the atmospheric or the vacuum distillation unit. In some cases, shell-side fouling not only occurs but it can be the dominant resistance to heat transfer. In such cases, neglecting the thermal and hydraulic effects of shell-side deposition may lead to gross errors in the analysis of plant data. The above-mentioned correlations relate fouling rates to tube-side conditions. As a result, when shell-side fouling is relevant, attributing all fouling to the tube side only results in the relationship between fouling rate and tube-side operating conditions not being captured correctly. The consequence is that thermal and hydraulic performance of the exchanger in the current state are incorrectly estimated and, more importantly, future states cannot be predicted correctly.

CONTACT Dr. Francesco Coletti f.coletti@hexxcell.com Hexxcell Ltd., Innovation Hub, Imperial College London, White City Campus, 80 Wood Lane, London W12 0BZ, UK.

Color versions of one or more of the figures in this paper can be found online at www.tandfonline.com/uhte.

© 2018 Taylor & Francis Group, LLC

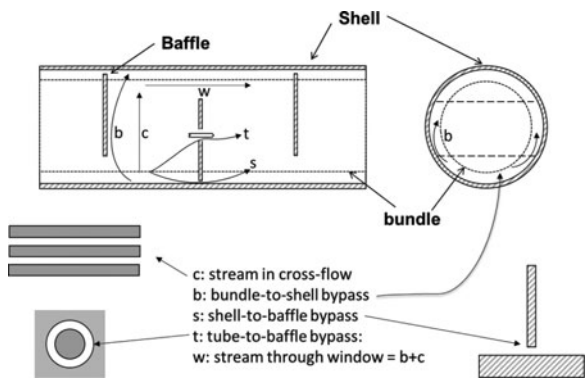

Figure 1. Shell-side flow streams.

Given its complex geometry, it is not easy to calculate thermal and hydraulic performance on the shell side. Tinker [14] proposed a method based on a "fluid flow fraction" concept whereby the effect of hydraulic resistances and dimensions for the different flow routes through the exchanger are taken into account (Figure 1); thus, the heat transfer coefficient and pressure drops are calculated as a function of geometrical parameters (baffle cut, baffle spacing, pitch angle, and length) and clearances (bundle-to shell, shell-top baffle, and tube-to-baffle).

Following the approach by Tinker [14], the Bell–Delaware [15], [16] and the Flow Stream Analysis [17] methods have been developed and are widely used in industry to calculate the thermal and hydraulic performance of the shell side *in clean conditions*. However, all the methods mentioned above do not take into account the effects of fouling buildup. Fouling affects the thermal and hydraulic performance of the shell side in two areas:

a) The outer surface of the tubes. As a result of the buildup on this surface, heat transfer with the inner side of the tube is impaired. Moreover, the reduction of the area available to the fluid flow increases the velocities in crossflow, thus increasing both convective heat transfer coefficient and pressure drops.
b) The shell clearances (bundle-to-shell, shell-to-baffle, and tube-to-baffle). While the heat exchanger is clean, the flow fractions through each clearance are determined by the geometrical clearances. As fouling builds up, these become occluded and the resistance to flow in the bypasses increase. As a result, the portion of crossflow – and with it the thermal and hydraulic performance of the exchanger – changes over time.

In his original paper, Tinker [14] already included some considerations on the effects of fouling on the clearances. He noted that baffle holes are likely to become completely plugged over an unspecified amount of time whilst other clearances may reduce to a certain percentage of the original clean geometry. He considered the case in which 80% of the flow passages have been restricted from the clean value. He noted that the increase in pressure drop as a result of this restriction was equivalent to increasing the flowrate by 25% in clean conditions. He suggested using a multiplier in the fluid fractions in order to adjust accordingly. Whilst this rule-of-thumb provides a practical way of estimating fouled pressure drops, it heavily relies on experience and does not take into account any dependence of fouling deposition on (usually variable) process conditions. As a result, it cannot be used to find designs that minimize fouling.

Whilst to the authors' knowledge there are no models that consider both effects described above, some limited attempts exist describing shell-side fouling. Clarke and Nicolas [18] presented a computational fluid dynamics model for an entire shell side of a heat exchanger where the fraction occupied by the tubes is accounted for as a time-varying porosity. Fouling, predicted using the threshold model by Ebert and Panchal [19], was used to gradually reduce porosity inside the shell. This approach allowed reducing the number of grid elements needed for the calculations (thus the computational power) on the shell side. However, the interactions between tube and shell sides were ignored. Vessakosol and Charoensuk [20] studied the heat transfer and flow patterns around a tube in crossflow (assumed to be laminar and steady-state) with fouling. The fouling layer was modeled as an annulus with constant thermal properties and various deposit conductivities and shapes of the fouling layer were investigated but the dynamics of deposition was neglected. Whilst these studies provide some insights into shell-side fouling, they require several difficult to measure parameters and are difficult to validate. Other research efforts focus on fouling on the outer surface of tube banks with simpler geometries, such as burners [21], [22].

In this paper, a new model that allows capturing fouling on the shell side of shell-and-tube heat exchangers is presented. Since, as discussed above, fouling growth is system specific (i.e., a function of fluids, local conditions, time, etc.), the results presented here are for a specific application to refinery crude preheat trains. However, the model can readily be generalized by replacing sub-model used for the crude oil fouling with other system specific ones (e.g., for water, milk, particulate, etc.). Nonetheless, the conclusions drawn for the industrial case study considered here are general and demonstrate the importance of considering shell-side fouling in order to correctly capture and predict the fouling behavior and performance of shell-and-tube heat exchangers. An earlier version of this paper was presented at the International Conference on Heat Exchanger Fouling and Cleaning – 2015 in Enfield (Dublin, Ireland) [23].

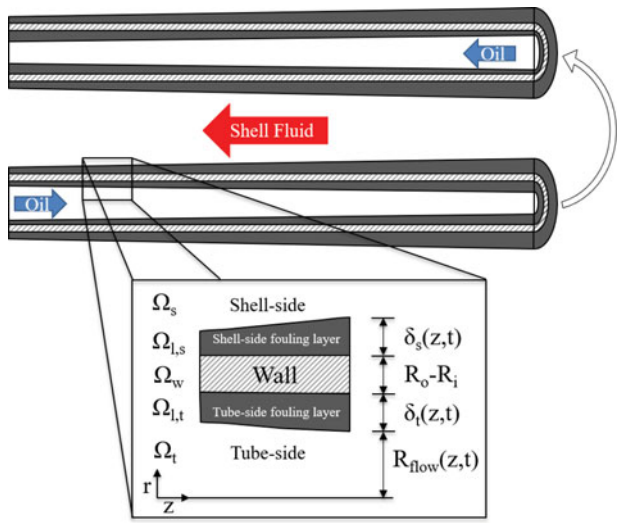

Figure 2. Schematic representation of a two-pass heat exchanger with inner and outer tube fouling.

Model description

The model for shell-and-tube heat exchangers undergoing crude oil fouling by Coletti and Macchietto [24] is extended here to consider fouling on the shell side. The original model by Coletti and Macchietto [24] is dynamic, distributed, and captures tube-side fouling as a function of local conditions in each pass. It comprises 4 spatial domains: shell-side flow (Ω_s), tube wall (Ω_w), tube-side fouling layer ($\Omega_{l,t}$), and tube-side flow (Ω_t). A new fifth domain is introduced here to represent a fouling layer building up on the outer surface of the tubes. The new configuration, including the shell-side fouling domain ($\Omega_{l,s}$), is schematically shown in Figure 2. Other extensions include the use of Flow Stream Analysis to calculate shell-side pressure drops as well as the inclusion of the hydraulic effects of headers and nozzles [25], [26]. The main equations are summarized in Table 1 [17], [24], [27]–[30]. The following sections describe the models used to capture fouling on the outer surface of the tubes and on the clearances.

Outer tube fouling model

The deposit layer, both in the inner and outer surface of the tube (tube-side and shell-side fouling, respectively), is described by the model by Diaz-Bejarano *et al.* [31]. The model, originally derived to simulate inside-tube fouling, is distributed over the axial and radial direction in each pass and has the ability to retain composition history at each point through the deposit following deposition of multiple fouling species, partial removal, and partial cleaning events. The growth dynamics of the fouling layer is described with the use of a moving boundary problem and a Lagrangian transformation of the space. Originally, the boundary was moving just inward from the surface of the tube. Here, the deposit model is generalized to enable simulation of fouling both inside and outside a tube.

The mass and heat balances, following a Lagrangian transformation of the space in the radial direction [31], are given by Eqs. (1) and (2) for a given pass number n, respectively:

$$\left(\frac{\partial c_{l,i}\left(z,\tilde{r}\right)}{\partial t}-\frac{\tilde{r}}{\delta\left(z\right)}\dot{\delta}\left(z\right)\frac{\partial c_{l,i}\left(z,\tilde{r}\right)}{\partial\tilde{r}}\right)=\sum_{j=1}^{NR}\nu_{ij}r_j\left(z,\tilde{r}\right) \tag{1}$$

$$\rho_l\left(z,\tilde{r}\right)C_{p,l}\left(z,\tilde{r}\right)\left(\frac{\partial T_l\left(z,\tilde{r}\right)}{\partial t}-\frac{\tilde{r}}{\delta\left(z\right)}\dot{\delta}\left(z\right)\frac{\partial T_l\left(z,\tilde{r}\right)}{\partial\tilde{r}}\right)=\frac{1}{r\,\delta(z)^2}\frac{\partial}{\partial\tilde{r}}\left(r\lambda_l\left(z,\tilde{r}\right)\frac{\partial T_l\left(z,\tilde{r}\right)}{\partial\tilde{r}}\right) \tag{2}$$

Table 1. Main equations in the shell-and-tube heat exchanger model by Coletti and Macchietto [24], as summarized in [30].

	Tube side (Ω_t)
Energy balance	$\frac{\partial(A_{t,n}(z)\rho_{t,n}(z)H_{t,n}(z))}{\partial t}=-\mathrm{dir}_{t,n}\frac{\partial(A_{t,n}(z)\rho_{t,n}(z)u_{t,n}(z)H_{t,n}(z))}{\partial z}+p_{t,n}(z)h_{t,n}(z)(T_{l,t,n}\vert_{r=R_{\mathrm{ffow},t,n}}(z)-T_{t,n}(z))$ $h_{t,n}(z)$ calculated by Sieder–Tate correlation [28]
Overall heat duty*	$Q=\dot{m}\int_{T_{\mathrm{in}}}^{T_{\mathrm{out}}}C_p(T)dT$
Pressure drop	$\Delta P_t=\Delta P_{\mathrm{Headers},t}+\sum_{n=1}^{N_p}(P_{t,n,\mathrm{in}}-P_{t,n,\mathrm{out}})-\mathrm{dir}_{t,n}\frac{dP_{t,n}(z)}{dz}=\frac{C_{f,n}(z)\rho_{t,n}(z)u_{t,n}(z)^2}{R_{\mathrm{ffow},t,n}(z)}=\frac{2\tau_{t,n}(z)}{R_{\mathrm{ffow},t,n}(z)}$ $C_{f,n}=f(\mathrm{Re}_{t,n})$ [27]
Shell side (Ω_s)	
Energy balance	$\frac{\partial(A_s\rho_s(z)H_s(z))}{\partial t}=-\mathrm{dir}_s\frac{\partial(A_s\rho_s(z)u_s(z)H_s(z))}{\partial z}+\sum_{n=1}^{N_p}p_{s,n}h_s(z)(T_s(z)-T_{l,s,n}\vert_{r=R_{\mathrm{ffow},s}}(z))h_s(z)$ calculated with Bell–Delaware method [29] ΔP_s calculated with Flow Stream Analysis [17]
	Tube wall (Ω_w)
Energy balance	$\rho_{w,n}C_{p,w,n}(z,r)\frac{\partial T_{w,n}(z,r)}{\partial t}=\frac{1}{r}\frac{\partial}{\partial r}(r\lambda_w\frac{\partial^2 T_{w,n}(z,r)}{\partial^2 r})$

*Calculated using either tube-side or shell-side data.

where $c_{l,i}$ is the mass concentration of component i, z the axial coordinate, $\tilde{r}$ the dimensionless radial coordinate, r the dimensional radial coordinate, t time, δ the deposit layer thickness, $\dot{\delta}$ the rate of change in thickness, r_j the rate of reaction j, T_l temperature, ρ_l density, $C_{p,l}$ specific heat capacity, and λ_l thermal conductivity of the mixture. The local thermal conductivity ($\lambda_{l,n}(z, \tilde{r})$) at each point of the layer varies over time and as function of local composition and transformations such as aging. The heat flux through the layer is defined as

$$q_l'' = \frac{-\lambda_l\left(z, \tilde{r}\right)}{R_{\text{flow}}\left(t, z\right) - R} \frac{\partial T_l\left(z, \tilde{r}\right)}{\partial \tilde{r}} \tag{3}$$

The dimensionless radial coordinate ($\tilde{r}$) is defined as

$$\tilde{r} = \frac{r - R}{R_{\text{flow}}\left(t, z\right) - R} \tag{4}$$

where R is the radius corresponding to the interface between tube wall and fouling layer, and R_{flow} is the radius corresponding to the interface between fouling layer and fluid, which varies as fouling builds up. The difference between inside and outside fouling relies on the definition of the reference radii (inner radius for inside tube fouling, R_i; outer radius for outside tube fouling, R_o). In both cases, $\tilde{r} = 1$ corresponds to the surface of the fouling layer (i.e., the interface with the fluid flow) and $\tilde{r} = 0$ corresponds to the wall surface.

The heat balance boundary conditions provide continuity to the heat flux and temperature radial profiles. At the interface between shell-side domain (Ω_s) and the shell-side deposit layer domain ($\Omega_{l,s}$),

$$q''_{l,s,n}\Big|_{r=R_{\text{flow},s}} = -h_s\left(T_s - T_{l,s,n}\Big|_{r=R_{\text{flow},s}}\right) \tag{5}$$

At the interface between the shell-side deposit layer domain ($\Omega_{l,s}$) and the wall domain (Ω_w),

$$q''_{l,s,n}\Big|_{r=R_o} = q''_{w,n}\Big|_{r=R_o} \tag{6}$$

$$T_{l,s,n}\Big|_{r=R_o} = T_{w,n}\Big|_{r=R_o} \tag{7}$$

Similarly, the boundary conditions at the interface between tube-side deposit layer domain ($\Omega_{l,t}$) and tube-side deposit layer (Ω_t) are

$$q''_{l,t,n}\Big|_{r=R_{\text{flow},t}} = -h_{t,n}\left(T_{l,t,n}\Big|_{r=R_{\text{flow},t}} - T_{t,n}\right) \tag{8}$$

The boundary conditions between tube-side deposit layer domain ($\Omega_{l,t}$) and the tube wall domain (Ω_w) are

$$q''_{l,t,n}\Big|_{r=R_i} = q''_{w,n}\Big|_{r=R_i} \tag{9}$$

$$T_{l,t,n}\Big|_{r=R_i} = T_{w,n}\Big|_{r=R_i} \tag{10}$$

Finally, at each axial location the local thermal resistances to heat transfer offered by the tube-side and shell-side deposits, referred to the outer tube area, are

$$R_{f,t,n}\left(z\right) = \frac{T_{l,t,n}\Big|_{r=R_{\text{flow},t,n}}\left(z\right) - T_{l,t,n}\Big|_{r=R_i}\left(z\right)}{q''_{w,n}\Big|_{r=R_o}\left(z\right)} \tag{11}$$

$$R_{f,s,n}\left(z\right) = -\frac{T_{l,s,n}\Big|_{r=R_{\text{flow},s,n}}\left(z\right) - T_{l,s,n}\Big|_{r=R_o}\left(z\right)}{q''_{w,n}\Big|_{r=R_o}\left(z\right)} \tag{12}$$

The average tube and shell fouling resistances ($R_{f,t,\text{av}}$ and $R_{f,s,\text{av}}$, respectively) are obtained by integrating Eqs. (11) and (12) along each pass and averaging for all passes. Finally, the overall fouling resistance (R_f) is calculated as the sum of the average tube and shell average fouling resistances.

Calculation of variables relevant to fouling deposition

The relationship between fouling rates and operating conditions is complex and depends on the dominant fouling mechanism. For chemical reaction in crude oil fouling, the film temperature and the wall shear stress are the two main operating conditions usually considered [2] (in milk fouling, these may include protein concentration, etc.). The film temperature is calculated locally for tube and shell sides as follows:

$$T_{\text{film},n}\left(z\right) = T_n\left(z\right) + 0.55\left(T_n\left(z\right) - T_{l,n}\Big|_{r=R_{\text{flow},n}}\left(z\right)\right) \tag{13}$$

The tube-side shear stress is calculated using the correlation by Saunders [27]. The shear stress in the shell side is difficult to calculate because of its complex geometry. On the other hand, the total loss of energy for crossflow through tube banks has been measured experimentally as a function of Reynolds number, leading to correlations (as functions of Re) for the drag coefficient for various bundle configurations [32]. For the shell side, the total force per unit of tube area (F/A) based on such correlations is used in this paper instead of the wall shear stress. The total force includes drag and skin friction.

Occlusion of clearances

As mentioned in the introduction, traditional shell-side calculations such as the Bell–Delaware [15], [16] and Flow Stream Analysis [17] consider the effect of leakage through clearances on heat transfer coefficients and pressure drops only in clean conditions. Here, the progressive occlusion of the clearances produced by fouling (schematically shown in Figure 3) is considered. Fouling

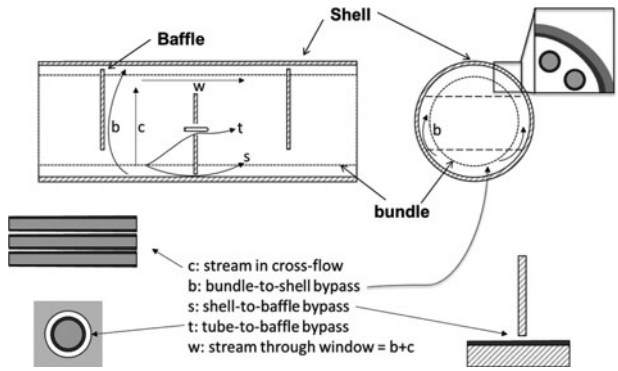

Figure 3. Flow streams in shell side and schematic representation of occlusion of clearances due to fouling, depicted as a black layer.

buildup on the inner surface of the shell is also considered. The latter does not affect directly the heat exchanged between fluids or between shell and the environment, but only the various clearances (bundle-to-shell and baffle-to-shell), thus flow redistribution and (indirectly) the shell-side heat transfer coefficient and pressure drop. This coupling is an important feature of the model.

The main assumptions are

(i) Clearances are uniform throughout the length of the heat exchanger, that is, occlusions are calculated for an average deposit thickness on the shell side.
(ii) Local flow patterns near the clearances are neglected.
(iii) Deposit thickness on the inner surface of the shell is equal to the average thickness on the outer tube surface.

The shell-side clearances under fouling conditions are defined as

$$\mathrm{Ltb}\ (t) = \mathrm{Ltb}_c - 2\delta_{s,\mathrm{av}}\ (t) \tag{14}$$

$$\mathrm{Lbb}\ (t) = \mathrm{Lbb}_c - 4\delta_{s,\mathrm{av}}\ (t) \tag{15}$$

$$\mathrm{Lsb}\ (t) = \mathrm{Lsb}_c - 2\delta_{s,\mathrm{av}}\ (t) \tag{16}$$

$$\mathrm{Ltt}\ (t) = \mathrm{pt} - 2\left(R_o + 2\delta_{s,\mathrm{av}}\ (t)\right) \tag{17}$$

where Ltb is the tube-to-baffle diametral clearance, Lbb the bundle-to-baffle diametral clearance, Lsb the shell-to-baffle diametral clearance, Ltt the space between adjacent tubes in the tube bundle, pt the pitch, $\bar{\delta}_s$ the average shell deposit thickness, and subscript c denotes clean conditions. These "fouled" clearances are implemented in the Bell–Delaware [15], [16] and Flow Stream Analysis [17] methods instead of the usual "clean" clearances.

Solution types

The model above has been implemented in Hexxcell Studio^{TM}, an advanced thermo-hydraulic fouling analysis and prediction software [33], which allows various solution types. Solution types refer to different ways of solving the model presented above, depending on the choice of degrees of freedom. Two solution types, for which the choice of degrees of freedom is summarized in Table 2, are used in this paper:

Analysis type: Fouling deposit characteristics are calculated over time as a function of measured inlet conditions of temperature and flowrate, heat duty calculated from primary measurements, and (when available) pressure drop measurements. That is, the evolution of the deposit is inferred directly from the data and no fouling deposition models are used. When this solution method is used, the deposit's characteristics (thickness, thermal conductivity) are uniform (no spatial distribution). These properties are referred to as *apparent*. In the absence of pressure drop measurements, and when shell-side fouling is negligible, an *apparent* tube-side deposit thickness ($\delta_{a,t}$) can be calculated by fixing the deposit thermal conductivity, allowing the use of the model as *soft* tube-side pressure drop sensor (see example in [34]). If shell-side fouling is nonnegligible, an additional assumption on the distribution of the fouling deposit is necessary to fulfil the one remaining degree of freedom of the mathematical system (now there is a new variable – the *apparent* shell-side deposit thickness, $\delta_{a,s}$ – and hence a new equation is required). Here, the approach is to assume a shell fouling-to-total fouling ratio, K_s, which may be constant or time-varying. The result is the calculation of tube-side and shell-side apparent thickness over time from plant measurements. The ratio may be defined in terms of deposit thickness or, as in this paper, in terms of thermal fouling resistance:

$$K_s = \frac{R_{f,s,\mathrm{av}}}{R_{f,s,\mathrm{av}} + R_{f,t,\mathrm{av}}} \tag{18}$$

In this solution type, the heat balance on the deposit (Eq. 2) applies, but the mass balance (Eq. 1) is not necessary.

Prediction type: The thermo-hydraulic performance of the exchanger is calculated over time as function of inlet operating conditions and deposit characteristics.

Table 2. Differences in choice of degrees of freedom and model configuration in a heat exchanger with tube-side and shell-side fouling.

Solution type	Analysis	Prediction
Inputs	$[T_{\mathrm{in}}, \dot{m}, \lambda_a]_{s,t}$, Q, K_s	$[T_{\mathrm{in}}, \dot{m}]_{s,t}$
Additional equations	[Eq. (18)]	[Eq. (19)]$_{s,t}$
Outputs	$[\delta_a, \Delta P, T_{\mathrm{out}}]_{s,t}$	Q, $[\Delta P, T_{\mathrm{out}}]_{s,t}$
HEX spatial distribution		Axial for each pass
Deposit spatial distribution	None	Axial and radial for each pass

Note: subscripts in, *s*, *t*, and *a* refer to inlet, shell, tube, and apparent

The deposit characteristics (thickness, thermal conductivity) are determined by the deposition rate of the various fouling species. The local rate of change in deposit thickness in pass n includes fouling and cleaning rates, both defined in terms of mass fluxes [31]:

$$\dot{\delta}_n(z) = (1-b)\sum_{i}^{NC}\frac{1}{\rho_i}n_{f,i,n}(z) - \sum_{k=1}^{NCl} b_k \frac{1}{\rho_{l,n}(z,1)} n_{Cl,k,n}(z) \quad (19)$$

where ($n_{f,i}$) is the net deposition rate of species i, $n_{Cl,k}$ is the cleaning rate of cleaning method k, b_{clean} is a 0–1 variable defining if any cleaning is taking place and b_k is a binary variable which indicates if cleaning method k is active ($b_k = 1$) or not ($b_k = 0$). The formulation above allows seamless simulation of fouling–cleaning sequences, as demonstrated in [31], [34], and [35] for theoretical and industrial case studies. Cleaning rate models have been proposed in those references to describe mechanical and chemical cleaning actions. Eq. (19) is applicable and is applied independently to both tube-side and shell-side deposits.

Method

The method for analysis of fouled exchangers plant data is based on the thermo-hydraulic analysis method by Diaz-Bejarano et al. [34]. The methodology used here comprises the following steps:

(1) *System definition, data filtering, and error analysis*: Model setup (geometry, fluid physical properties) and pretreatment of available plant data, if required.
(2) *Dynamic analysis of fouling state*: Fouling state refers to the extent and properties of the deposit (e.g., conductivity profiles). The analysis solution type of the model is used to obtain information on the extent of fouling, identify cleaning actions, obtain preliminary insights into the impact of fouling on the system's hydraulics, and investigate the range of deposit conductivity that leads to reasonable blockage of the flow area.
(3) *Selection of deposition rate model*: A suitable deposition rate model is selected. The functionality in the deposition rate determines the growth of the deposit in tube and shell sides over time and along the exchanger.
(4) *Estimation and testing of fouling parameters*: The unknown parameters in the selected deposition model are estimated by using the measured time varying inlet temperatures and flowrates as inputs to the heat exchanger model and fitting the measured outlet conditions. The parameter estimation method uses a maximum likelihood approach [36]. In this paper, the estimation is performed by fitting measured outlet temperatures.

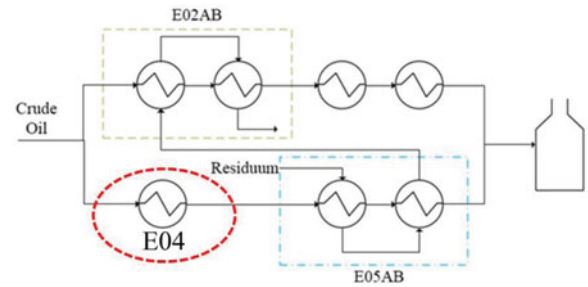

Figure 4. Location of E02, E05, and E04 in the network (adapted from [34]).

Case study

The case study involves a single-shell heat exchanger at the hot end of a refinery preheat train. The location of the exchanger under study, E04, is shown within a dashed circle in the simplified flow diagram in Figure 4, where two other multipass, double-shell heat exchangers, E02AB and E05AB, are also indicated with rectangular boxes. Those double-shell heat exchangers were analyzed in a previous work [34] with tube-side fouling models fitted to plant data and successfully tested in prediction mode for a period of over 1,000 days. Shell-side fouling was reported to be negligible.

The objective of the present case study is to analyze the fouling behavior in E04 where, as discussed below, fouling is significant on both tube and shell sides.

Results

System definition, data filtering, and error analysis

The main parameters related to the heat exchanger geometry and the physical properties of the fluids are reported in Table 3. The physical properties of the fluids (C_p, λ, μ, ρ) are calculated locally and over time as function of temperatures and the characteristic parameters in the table by means of well-established correlations [37].

The set of plant data comprises inlet temperature, outlet temperature, and flowrates for both fluids over a period of 1,174 days of operation, for which average daily data are available. The range of operation for each of those measured variables is also reported in Table 3.

Table 3. Main geometric parameters, fluids physical properties parameters, and operation ranges for E04.

Parameter	Value	Parameter	Tube fluid	Shell fluid
N_s	1	Fluid	Crude oil	Distillation product
N_p	4	API	35	26.4
L [m]	6.1	MeABP [°C]	232.6	400
D_s [mm]	1270	$\nu_{38°C}$ [mm^2 s^{-1}]	5.5	30
D_i [mm]	19.86	T range [°C]	164–227	194–335
D_o [mm]	25.4	$\dot{m}$ range [kg/s]	60–130	4–28
N_t	890			
Lbb_c [mm]	50.8			
Ltb_c [mm]	0.8			
Lsb_c [mm]	4.76			
Ltt_c [mm]	6.35			

Data with gross errors were filtered out, as in [34]. The residual error remaining in the heat balance, associated to errors in the measurements and the calculated physical properties, is within ±10%. The heat duty used as input in the analysis of fouling state is taken equal to the average between that calculated only with tube-side measurements and that calculated only with shell-side measurements. If the measured inlet conditions are assumed to be correct, the error in the heat balance translate into errors on the outlet temperatures (in °C) of ±1% and ±5% for the tube and shell sides, respectively. The error associated to the shell side is greater because of the much lower flowrate. These errors are used later to evaluate the quality of the estimation and predictions.

Dynamic analysis of fouling state

The dynamic analysis of fouling state of E04 revealed the overall fouling resistance shown in Figure 5. This is an *apparent* R_f, as it does not consider the spatial distribution of fouling along the exchanger. Three periods in-between mechanical cleanings (P1, P2, P3) are clearly identified for E04. The mechanical cleanings are not completely effective. The overall resistance after cleaning is in the range 2–3 m^{2}K^{-1} kW^{-1}. Operating periods P1 and P3 show similar fouling behavior, with initial fast fouling buildup and a falling rate change after reaching $R_f \approx 1.3$–1.5 m^{2}K kW^{-1}. The fouling behavior seems to be different in period P2, when an almost linear fouling behavior is observed, reaching values of $R_f \approx 2$ m^{2}K kW^{-1} in 200 days. That value is only reached after ≈400 days in the other periods.

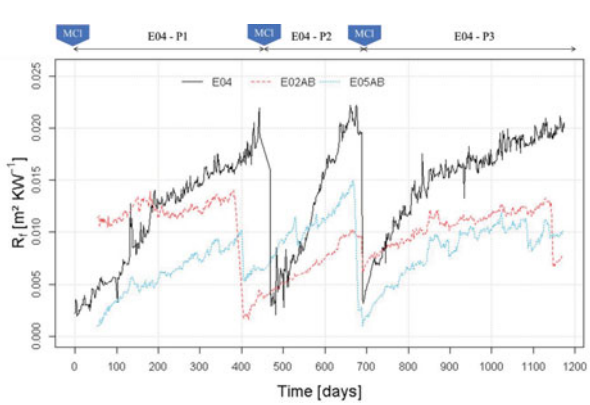

Figure 5. Overall fouling resistance referred to outer tube area for E04, E02AB, and E05AB, obtained from dynamic analysis of fouling state. MCI indicates mechanical cleaning of E04.

The fouling resistances in E05AB and E02AB are also shown in Figure 5. As discussed in [34], three periods in-between cleanings can also be defined for those exchangers. The data for E05AB starts just after a mechanical cleaning. After 400 days, it undergoes a chemical cleaning. Finally, it is mechanically cleaned after approx. 690 days, coinciding with the last mechanical cleaning of E04. The data for E02AB starts under fouled conditions. A mechanical cleaning was performed after 400 days (coinciding with the chemical cleaning of E05AB), and a chemical cleaning was performed after 690 days (coinciding with the second cleaning of both E04 and E05AB.

E02AB and E05AB, with very similar tube-side design to E04, were reported to undergo tube-side fouling only. By comparison of periods with similar operation history, the fouling resistance in E04 is roughly twice that in E05AB and E02AB. This difference could be the result of significant shell-side fouling in E04, not happening in the other units. Based on the above observations, a value of $K_s = 0.5$ was used in the analysis of fouling state of E04, that is, 50% of the fouling resistance is assumed to be allocated on the shell side.

The next step is to establish the range of feasible thermal conductivities. The approach consists in carrying out a sensitivity analysis on the deposit conductivity and identify the range of values for which the results are feasible. The conductivity of organic-rich crude oil deposits is typically around 0.2 W/mK [38]. This conductivity may increase over time at high temperature due to aging [12], or be higher from the start if significant amount of inorganic materials are present in the deposit [39]. The range of conductivities explored in the sensitivity analysis covered values from 0.2 W/mK and above.

The range of tube-side deposit conductivity was found to be 0.2–0.4 W/mK for E02AB and E05AB in a previous work [34]. This range was determined by analyzing the impact of fouling on the tube-side pressure drop. It was assumed that the same thermal conductivity range applied to the E04 tube-side deposit.

Following a similar approach, a sensitivity analysis on the shell-side deposit conductivity was performed for E04. Figure 6 shows the apparent shell-side deposit thickness $\delta_{s,a}$ in period P1 for the assumed $K_s = 0.5$ and three values of shell-side deposit conductivity ($\lambda_{l,s}$). The feasibility of

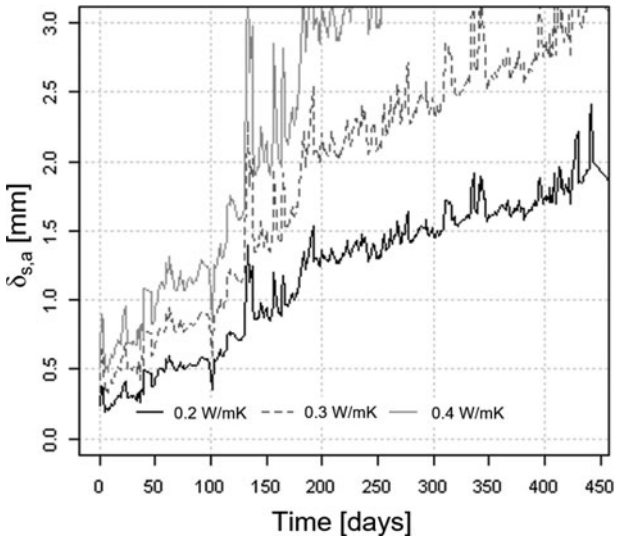

Figure 6. Apparent shell-side deposit thickness, $\delta_{s,a}$, in E04 during Period 1, for $K_s = 0.5$ and three values of shell-side thermal conductivity ($\lambda_{l,s}$). The maximum physically allowed deposit thickness is 3.175 mm.

the conductivity values is assessed against the maximum allowed thickness, which corresponds to half the distance between adjacent tubes, that is, $Ltt_c/2 = 3.175$ mm. As observed in Figure 6, the maximum thickness is reached before 200 days for $\lambda_{l,s} = 0.4$ W/mK, and toward the end of period P1 for $\lambda_{l,s} = 0.3$ W/mK. On the other hand, the apparent thickness stays in values below 2.5 mm throughout the whole period P1 for $\lambda_{l,s} = 0.2$ W/mK. It is concluded that the conductivity of the shell-side deposit must be around $\lambda_{l,s} = 0.2$ W/mK, as greater values lead to physically unfeasible solutions.

The operating conditions inside the heat exchangers were then calculated using the models, with tube-side deposit conductivities $\lambda_l = 0.2$ W/mK for all exchangers, and shell-side deposit (E04 only) with shell-to-tube conductivity ratio $K_s = 0.5$. Figure 7(a) shows the average tube-side film temperature against the average tube-side wall shear stress at the deposit surface over time for E04, E02AB, and E05AB in period P1, obtained from the dynamic analysis of fouling state. Each dot in the graph represents (average) conditions in each exchanger on a particular day. The time evolution is indicated by a color transition from darker, for older data, to paler colors, for newer data. E05AB and E04 evolve over time toward higher shear stress, as a result of fouling build up. E02AB barely evolves, as it was already quite fouled at the start of P1 and fouling barely increases during this period. The graph indicates that the operating conditions on the tube side are very similar in the three exchangers, particularly with respect to shear stress. The results reinforce the hypothesis of similar tube-side fouling behavior in the three exchangers.

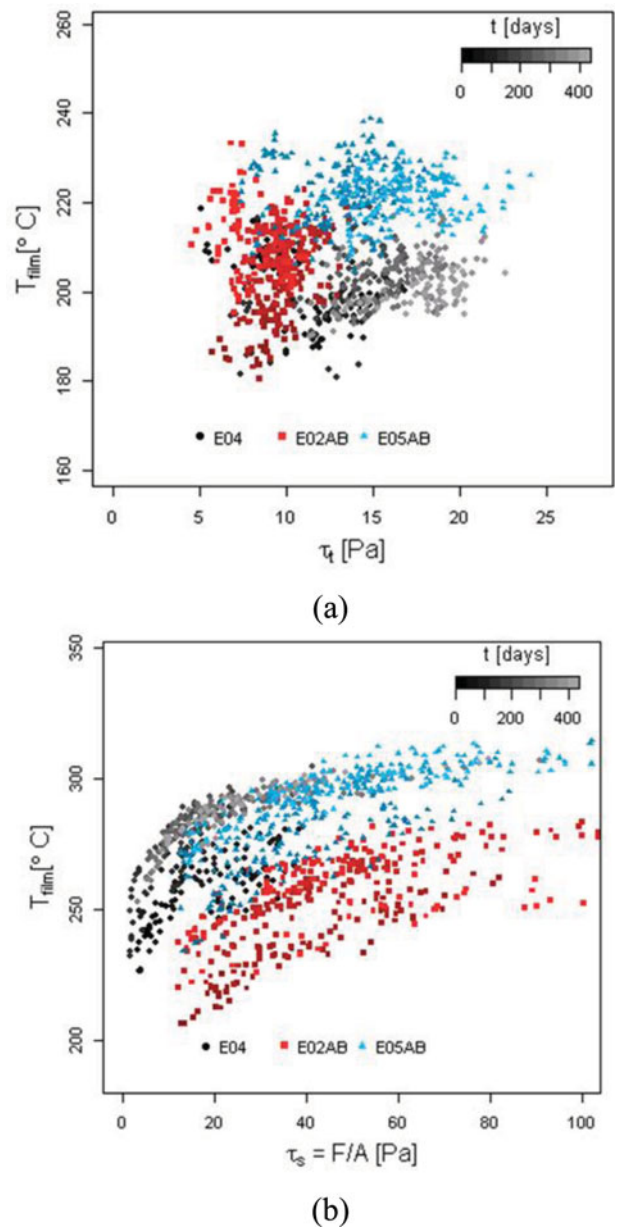

Figure 7. Average film temperature against shear stress on the tube side (a) and against total forces per unit of area on the shell side (b) over time in period P1 in E04, E02AB, and E05AB. Lighter dots correspond to later times.

Figure 7(b) shows the equivalent graph for the shell side, where total force per unit area is used on the abscissa instead of shear stress (as defined in the Model Description section). In E02AB and E05AB, the total forces vary over a much wider range (no lower than 15 Pa). The variation is similar in both exchangers and is mainly due to changes in the shell-side flowrate, which is the same for both exchangers. On the other hand, E04 starts at very low total forces, well below 15 Pa, which increase with fouling buildup, reaching values in the ballpark with E02AB and E05AB at long times. The much lower forces in E04

compared to the other exchangers would explain the significant buildup of shell-side fouling and reinforces the hypothesis of combined shell-side and tube-side fouling in E04.

Selection of deposition rate models

The deposition rate is assumed to be caused by a single fouling species and is calculated (at each point and local conditions) using the functional form of the threshold fouling model by Panchal *et al.* [40], for both tube and shell sides:

$$n_{f,n}(z) = \alpha' \, \mathrm{Re}_n(z)^{-0.66} \underset{n}{\mathrm{Pr}}(z)^{-0.33} \, exp\left(\frac{-E_f}{\mathrm{RT}_{\mathrm{film},n}(z)}\right) - \gamma' \tau_n(z) \quad (20)$$

where α', E_f, and γ' are fitting parameters. As noted in the Model Description section, the total forces instead of the shear stress are used on the shell side. The implicit assumption in the calculation of the shell-side fouling rates is that both drag (turbulence) and friction affect the removal term (negative term in Eq. 20).

As discussed in [34], and based on the feasible conductivity range, the fouling mechanism on the tube side is most likely due to deposition of organic matter, as expected for exchangers located at the hot end, with negligible or moderate aging. The tube-side deposit is assumed to be composed of two pseudo-components: fresh organic deposit ($\lambda = 0.2$ W/mK), which deposits according to Eq. (20), and, once it is settled, slowly transforms into coke ($\lambda = 1$ W/mK) due to aging (the only reaction considered). The rate of aging is

$$r_{a,n}\left(z, \tilde{r}_l\right) = A_a \, \exp\left(-\frac{E_a}{R_g T_{l,n}\left(z, \tilde{r}_l\right)}\right) c_{l,\mathrm{gel},n}\left(z, \tilde{r}_l\right) \quad (21)$$

where A_a and E_a, are fitting parameters. Several sets of parameters, corresponding to different aging rates, were obtained for E05AB and are reported in [34]. The set with very slow aging was found to provide excellent results in estimation (performed with period P1 data) and in prediction (over periods P2 and P3). This set is therefore used to describe tube-side fouling in E04. The selected tube-side fouling and aging parameters are shown in Table 4.

Table 4. Tube-side fouling and aging parameters [34].

	Parameter	Value
Deposition	α'_t (kg m^{-2} s^{-1})	1.00
	$E_{f,t}$ (kJ mol^{-1})	28.5
	γ'_t (kg m^{-2} s^{-1} Pa^{-1})	$3.6 \cdot 10^{-9}$
Aging	$A_{a,t}$ (s^{-1})	0.0015
	$E_{a,t}$ (kJ mol^{-1})	50

Based on the results in the previous section, the conductivity of the shell-side deposit must be, at most, 0.2 W/mK. A single pseudo-component with a characteristic conductivity $\lambda = 0.2$ W/mK is assumed, constant over time and not affected by any chemical reaction (the aging parameter $A_{a,s} = 0$, thus $r_{a,s} = 0$ and right hand side of Eq. (1) equals zero). The shell-side deposition parameters (α'_s, $E_{f,s}$, and γ'_s) are unknown and need to be estimated from plant data.

Estimation and testing of fouling parameters

Parameter estimation

As demonstrated in [23], the simultaneous and unambiguous estimation of tube-side and shell-side fouling parameters for a single heat exchanger based only on temperature measurements, although found often in literature, is not mathematically possible, as the thermal performance of the unit can be explained by multiple distributions of fouling between tube and shell sides. In that paper, the use of pressure drop measurements was pointed out as a possible solution to decouple shell and tube fouling. Here, we take advantage of the different fouling behavior in adjacent units to decouple the two. As detailed in previous sections, the tube-side parameters could be fixed to known values, estimated independently for adjacent exchangers, and the only estimation left from E04 data is that of the shell-side fouling parameters.

For consistency with [34], the estimation of the shell-side fouling parameters was performed using data for the entire period P1 (445 days). Inlet conditions are fixed at each time to the measured values and the model is fitted to the outlet temperatures. An initial deposit thickness was imposed in both tube and shell sides to provide an initial thermal resistance consistent with Figure 5. The parameter estimation results are shown in Table 5. Figure 8 shows the residuals of the simulated outlet temperatures ($\boldsymbol{T}_{\mathrm{out}}^{\mathrm{sim}}$) vs. plant measurements ($\boldsymbol{T}_{\mathrm{out}}$), calculated according to Eq. (22):

$$\mathrm{Residual}\,[\%] = \frac{T_{\mathrm{out}}^{\mathrm{sim}} - T_{\mathrm{out}}}{T_{\mathrm{out}}} 100 \quad (22)$$

The estimation was carried out successfully producing an excellent fitting of the measured outlet temperatures.

Table 5. Parameter estimation results for shell-side fouling in E04-Period 1.

Parameter	Value
α'_s (kg m^{-2} s^{-1})	0.12
$E_{f,s}$ (kJ mol^{-1})	27.2
γ'_s (kg m^{-2} s^{-1} Pa^{-1})	$1.32 \cdot 10^{-8}$

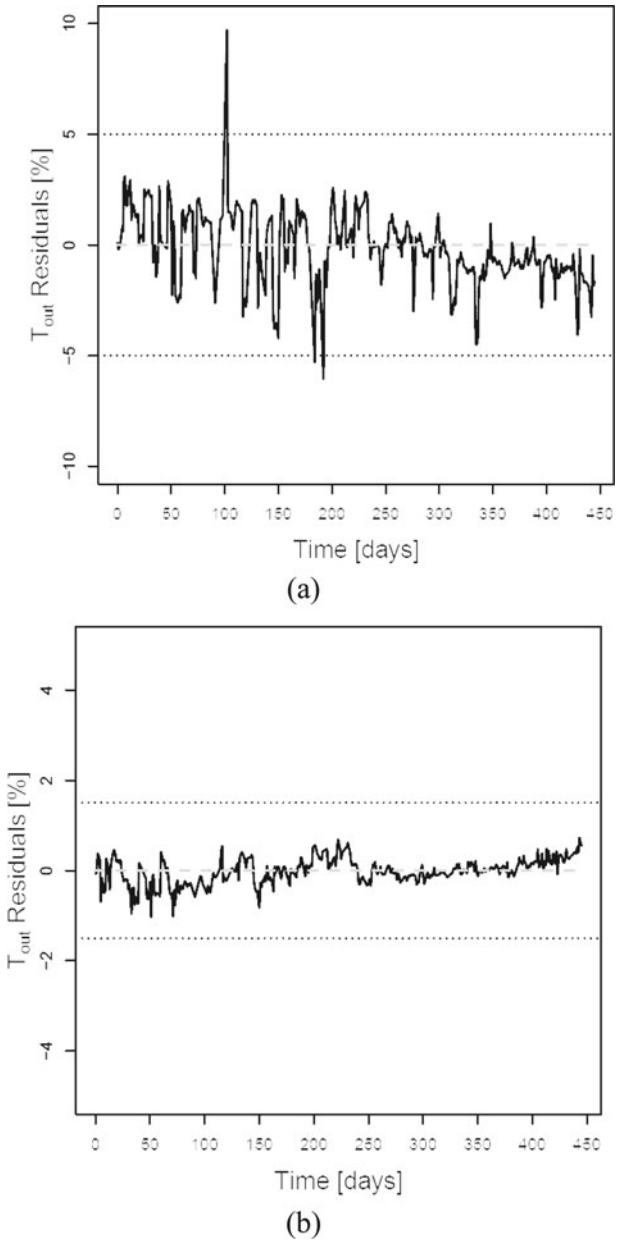

Figure 8. Residuals for shell (a) and tube outlet temperature (b) in the estimation of the shell-side fouling parameters for E04-Period 1. Horizontal dotted lines indicate measurement uncertainty.

The calculated temperatures are well within the uncertainty of the measurements defined in a previous section and reasonably well distributed.

Deposit thickness and occlusion of clearances

Figure 9a shows the evolution of the average deposit thickness (δ) on E04 tube and shell sides over time in period P1 (E04-P1). The tube-side thickness presents a monotonic increasing trend, with some changes in trend resulting from changes in inlet operating conditions. The shell-side thickness, on the other hand, presents an overall increasing but non-monotonic time profile. The

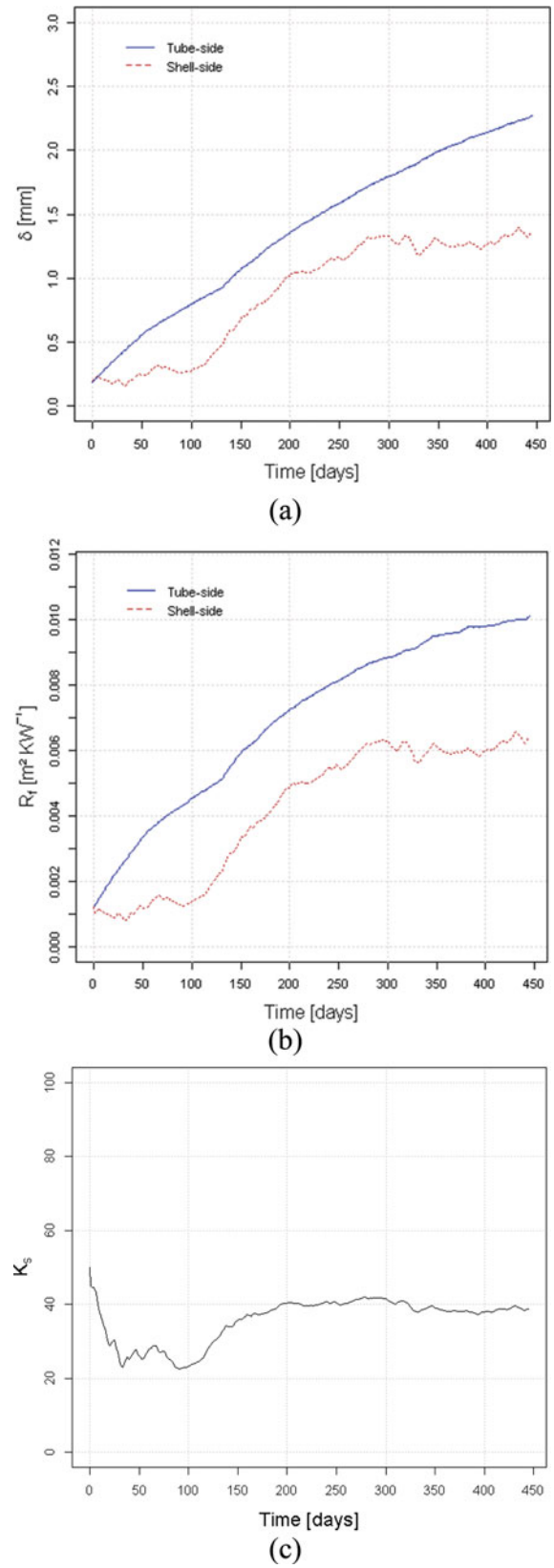

Figure 9. Average deposit thickness (a), average fouling resistance over time (b), and shell fouling-to-total fouling ratio in E04-P1 for tube and shell sides.

deposition rate on the shell side is more sensitive to changes in shear, thus in flowrate, resulting in periods with flat or even decreasing thickness coinciding with periods of high flowrate. The shell-side deposit thickness reaches a plateau after about 300 days, whilst the tube-side thickness continues increasing till the end of the operating period.

Figure 9b shows the average fouling resistance on tube and shell sides. The shell-side resistance presents a similar shape to the corresponding thickness, as the conductivity is constant. The tube-side deposit, on the other hand, presents an asymptotic trend, as a result of the gradual increase in conductivity due to aging. The fouling distribution between tube and shell sides varies over time (Figure 9c), as expected. At the end of the period, 40% of the resistance is on the shell side. This value is lower than the value of K_s assumed in the preliminary dynamic analysis step. Still, the results confirm the conclusions from that step of the existence of shell-side fouling and estimation of a suitable thermal conductivity.

In multipass exchangers, it is important to know not just what is the average deposit, but also, possibly, its location. This is an additional output of the analysis, as the growth of the layers is, according to the model, a function of the local conditions. The deposit thickness on both tube and shell sides for each pass at the end of Period 1 is shown in Figure 10a. The longitudinal variation of the deposit thickness is more relevant for the shell side following the larger temperature gradient experienced by the fluid on this side of the exchanger. The temperature gradient varies over time as a result of fouling dynamics. At the beginning, when the exchanger is almost clean, the shell-side fluid cools down until reaching the same outlet temperature as the tube-side fluid (Figure 10b). At that stage, the temperature decrease in the hot fluid is over 100°C. As fouling builds up, the thermal resistance impedes heat transfer and the hot fluid leaves at higher temperature. At the end of the period, the temperature decrease in the hot fluid is only 50°C (Figure 10c). The thicker portion of the shell-side deposit (Figure 10a) reaches high values (≈2.5 mm) but still less than the 3.175-mm limit imposed by the bundle geometry. The results confirm that the selected shell-side conductivity gives outcomes in line with the observed performance. This analysis is not possible if simpler lumped models are used to describe fouling dynamics.

One useful feature of the model is its ability to capture the effect of fouling on the shell-side clearances. Figure 11 shows that the tube-to-baffle clearance (Ltb) becomes completely blocked after 120 days of operation. The rest of the clearances, except shell-to-bundle, are also reduced significantly (by 40–50% after 1 year). The shell-to-bundle clearance (Lsb) in this heat exchanger is large, and therefore, in relative terms, fouling does not impact the flow significantly.

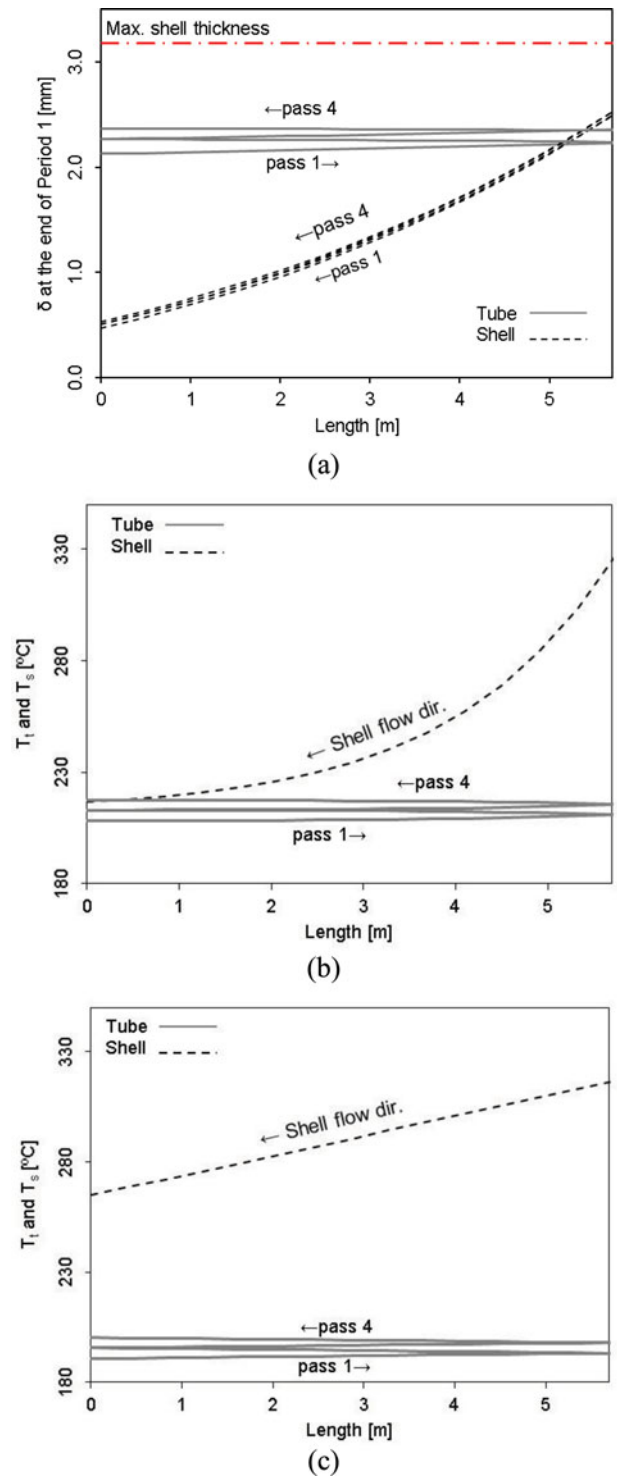

Figure 10. Axial distribution of deposit thickness at the end of period P1 (a), bulk temperature at the start of P1 (b), and bulk temperature at the end of P1 in E04 for tube and shell sides.

Model simulations enable quantifying the variations in the flow fractions inside the shell side due to the gradual occlusion produced by fouling (Figure 12). At the start of period P1, leakages account for 39% of the total

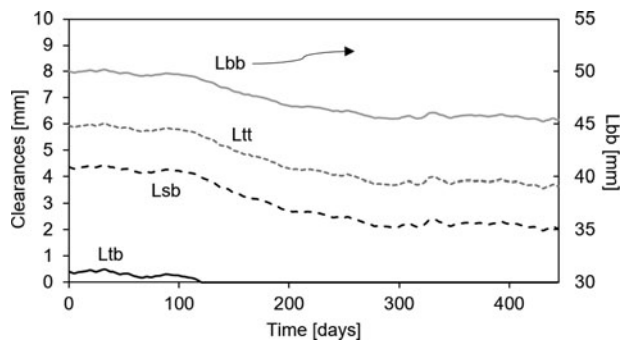

Figure 11. Occlusion of clearances due to fouling in E04-Period 1.

flow. As fouling builds up, the flow distribution on the shell side changes. In the early stages the tube-to-baffle clearance becomes blocked and the corresponding leakage is diverted to the other flow paths. As the hydraulic resistance for shell-to-baffle becomes important, the flow tends to go through the shell-to-bundle bypass area and the cross-flow area instead. At the end of the period, the crossflow and shell-to-bundle account for 70% and 23% of the flow fraction, respectively.

Thermo-hydraulic impact of shell-side fouling

In this section, the impact of the outer tube fouling on shell-side heat transfer coefficients and pressure drop is investigated in further detail. Shell-side fouling, as described here, has two main effects on the thermal performance of the heat exchanger: i) it decreases the overall heat transfer coefficient, hence reducing the heat transfer rate; ii) it increases the Reynolds number in crossflow, hence enhancing the convective heat transfer coefficient and promoting suppression/removal mechanisms. In order to understand the importance of the latter effect, the cases in which fouling affects the outer tube heat transfer with or without affecting the clearances are compared.

Figure 13 shows the shell-side heat transfer coefficient over time when considering and neglecting clearance

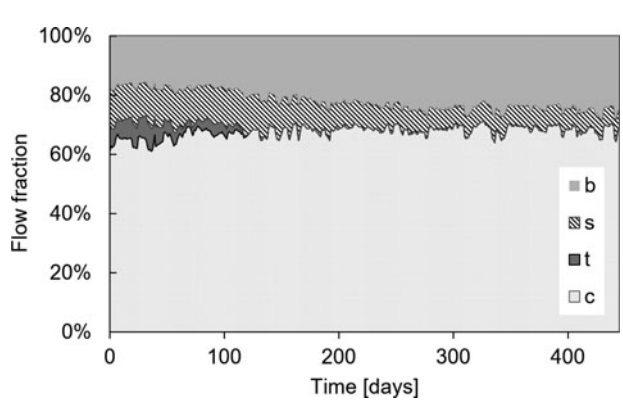

Figure 12. Time evolution of flow fraction through shell-side paths due to fouling in E04-P1. Labels b, c, s, and t indicate flow streams (see Figure 3).

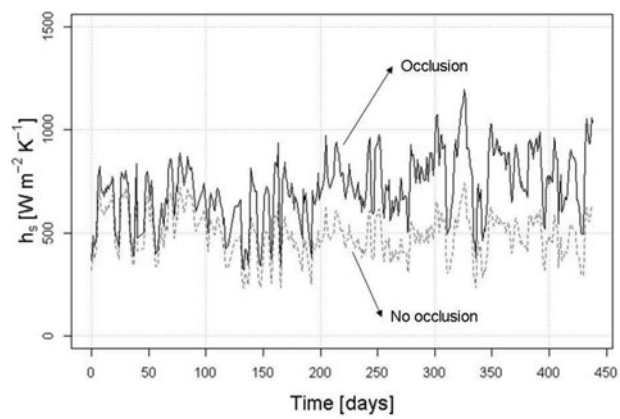

Figure 13. Shell-side heat transfer coefficient over time with and without occlusion of clearances in E04-P1.

occlusion. When no occlusion is considered, the coefficient simply fluctuates in accordance with flowrate and temperature variations. When the effect of occlusion is considered, the heat transfer coefficient increases significantly as fouling progresses (up to 50–80% at the end of P1). The gradual increase in Reynolds number, produced by the progressive restriction of the flow area and the increased cross-flow fraction generated by the blockage of the clearances, partly offsets the decrease in heat transfer due to fouling deposition.

Figure 14 shows the time evolution of the average total force per unit of tube area, considering and neglecting the impact of shell-side fouling on clearances. When the clearance occlusion is considered the space available for flow between tubes decreases leading to higher shear stress and drag forces, thus reduced fouling rate. Considering or neglecting the occlusion of clearances will no doubt affect the value of the deposition parameters at the estimation stage.

In terms of the hydraulic performance, the occlusion of clearances leads to significant increases in pressure drop over time (Figure 15): the pressure drop is doubled after

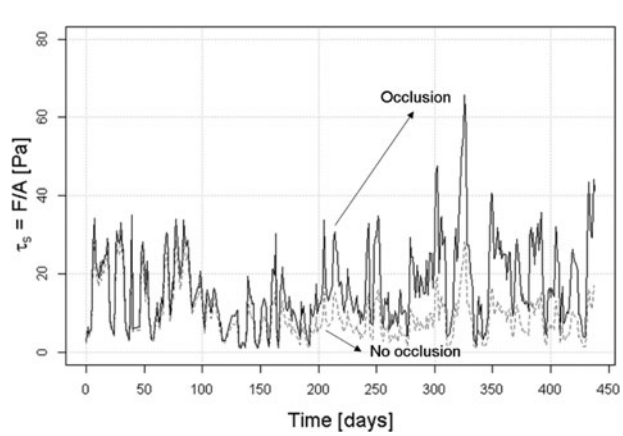

Figure 14. Shell-side forces per unit area over time with and without occlusion of clearances in E04-P1.

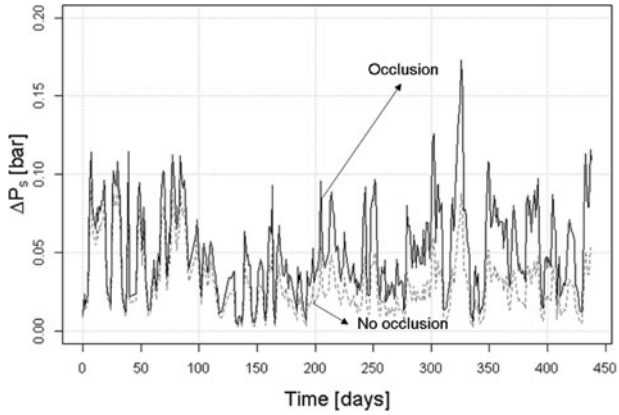

Figure 15. Shell-side pressure drop over time with and without occlusion of clearances in E04-P1.

a year of operation. Nevertheless, sensitivity of pressure drop on fouling is not as significant as in the tubeside, because of the availability of multiple flow paths for flow redistribution.

Testing the predictive capabilities of the model

With deposition parameters fitted during period P1 and now completely fixed, the predictive capabilities of the model were tested by comparing the model prediction to measurements for the subsequent operating periods, P2 and P3. A seamless simulation of the full fouling–cleaning sequence (Period 1 – Cleaning – Period 2 – Cleaning – Period 3) was run for E04, with tube-side and shell-side deposition parameters fixed to those in Tables 4 and 5, respectively. The cleanings were simulated as described in [31]. The cleaning terminates when the overall fouling resistance is restored to the initial value obtained for each period in the dynamic analysis of fouling state (Figure 5). The simulation involves 1,174 days of operation, of which 445 days correspond to the estimation period (Period 1), while the next 729 days (2 years ahead) are simulated in fully predictive mode. As before, the inlet temperature and flowrates on both shell and tube sides were set to the daily values measured in the refinery and predictions quality was assessed by comparing predicted and actually measured exit temperatures.

The outlet temperature residuals are shown in Figure 16a,b. The predicted fouling trend is also visualized in terms of the average overall fouling resistance, R_f, shown in Figure 16c, where it is compared to the apparent R_f obtained in the preliminary dynamic analysis. In period P2, the results show good agreement over the first half of the period, with the residuals within the uncertainty of the measurements. After 550 days, however, there is a small deviation to residuals outside the measurement uncertainty. However, even in this half period residuals are still on average just around 6–7% under-prediction, with just some peaks around 10%. In

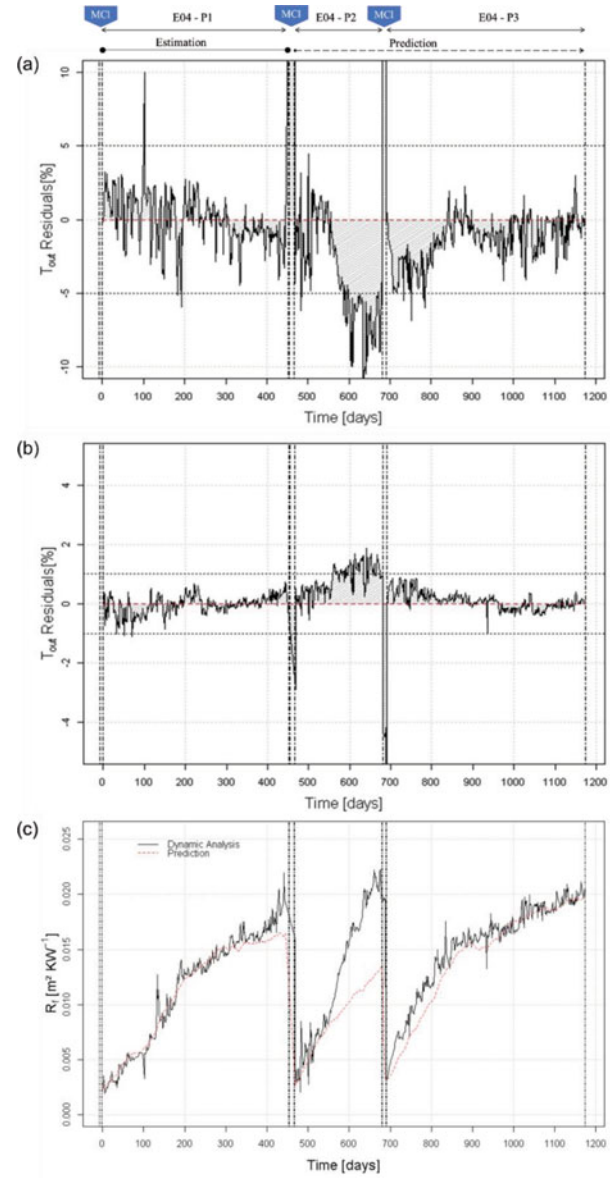

Figure 16. Seamless simulation of E04 operation schedule (periods P1-P2-P3). Outlet temperature residuals on the shell (a) and tube sides (b), and predicted average fouling resistance compared to that obtained in the dynamic analysis of fouling state (c) from Figure 5. MCI indicates mechanical cleaning of E04. Horizontal dotted lines indicate measurement uncertainty. Vertical dotted lines indicate start-end of cleaning actions.

period P3, the model predictions show excellent agreement with the measurements. The residuals are higher at the beginning but still within the uncertainty of the measurements, and very low after 850 days, at the same level of quality as in the estimation period.

These results are consistent with the analysis of E05AB in the same network and operating periods, previously reported in [34]. The residuals for E05AB, shown in Figure 17, present a similar pattern over period P2. The model is able to predict accurately the first half of the period, but the residuals start to deviate in the second

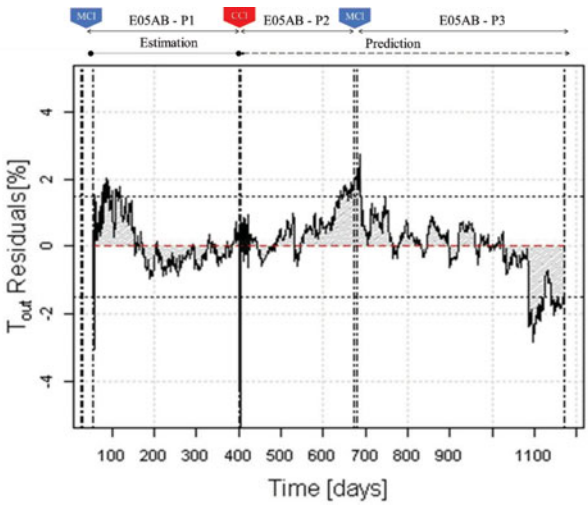

Figure 17. Seamless simulation of E05AB operation schedule (P1-P2-P3). Outlet temperature residuals on tube-side. MCI indicates mechanical cleaning and CCI indicates chemical cleaning. Adapted from [34].

half to values outside the measurement uncertainty. In the authors' experience the most likely cause of the mismatch in second half of P2 is a change in slate. This feature enables utilizing the models for monitoring and detecting other changes that may be affecting the unit fouling behavior (e.g., such as the processing of problematic oils, maloperation of upstream desalter).

Periodic re-estimation of some parameters, utilizing data and operating history as they develop, as opposed to just once, could possibly improve forward predictions even further.

Conclusions

In this paper, a model for shell-side fouling in refinery heat exchangers has been presented. To the authors' knowledge this is the first time that the effects of shell-side fouling buildup on heat exchange, shell-side heat transfer coefficient, and pressure drop are described taking into account, simultaneously, deposition on the outer tube surfaces and the progressive blockage of the shell-side clearances. The model is dynamic and distributed and considers the interaction of tube-side and shell-side local fouling rates. It was implemented within the Hexxcell Studio^{TM} simulation environment and, unlike computational fluid dynamics type models, may be used in simulations, monitoring, and predictions of heat exchanger networks as well as of individual exchangers.

The model and a novel method for using it have been applied here to an industrial case study involving a multipass, single-shell heat exchanger at the hot end of a refinery preheat train. The first question addressed is whether shell-side fouling should be considered at all. Based on a *dynamic analysis of the fouling state*, using a preliminary (time varying) tube to shell deposit conductivity ratio and by comparison with other nearby units in the same network, it was concluded that the heat exchanger undergoes significant fouling on both tube and shell sides. A feasible range for the conductivity of the shell deposit is obtained by a sensitivity analysis of the shell-side deposit thickness to its conductivity, and by comparing the results to a maximum allowable thickness identified based on the exchanger geometry. This first step is key to adequately defining the likely characteristics of the deposit and selecting the deposition model to be used in the next step to describe the fouling dynamics.

In a second step, the shell-side fouling deposition model is fitted to plant data. The case study used historical data covering 445 days of operation, sufficiently long to cover a variety of crude oils. The tube-side fouling parameters were assumed to be the same as those obtained for the surrounding exchangers in a previous work [34]. This strategy allowed the independent estimation of tube-side and shell-side fouling from just temperature and flowrate data. In this estimation period, results show that the model was able to predict the measured outlet temperatures within the estimated accuracy of the measurement for essentially all of the operation period considered. This step produces a comprehensive analysis of the state of the exchanger at the end of the estimation period (*current* state) and during the period, including shell-side deposit extent and location, occlusion of clearance, impact on heat transfer and pressure drop on both sides and overall thermal and hydraulic performance.

The model was then tested in fully *prediction* mode over the next two periods, covering 729 days of operation and two intermediate cleanings. The results demonstrate that, by combining tube-side and shell-side fouling and considering both as function of local operating conditions, the model has an excellent ability to accurately predict the fouling behavior of a unit over a very long-time horizon. The model was able to predict the measured outlet temperatures within the estimated accuracy of the measurement for most of the operation period considered and across cleanings. In practice, this gives confidence in the application of this predictive approach for applications such as evaluation of the economic impact of fouling, predictive maintenance, cleaning scheduling and optimization. One such example of industrial application to test alternative retrofit options was presented by Diaz-Bejarano *et al* [41].

Finally, the case study has been also used to illustrate the ability of the model to simulate shell-side fouling buildup along the heat exchanger, the gradual occlusion of shell-side clearances, the re-distribution of shell-side flow through available paths, and the impact of all these

processes on the shell-side heat transfer coefficient and pressure drop.

The case study presented in this paper related to crude oil fouling, however the model and methods illustrated apply to other cases, such as milk or crystallization fouling, with no or minimal adaptations.

Further validation of the model would require shell-side pressure drop measurements and comparison of model predictions with field observations of the state of the clearances upon dismantling of the heat exchangers at the end of operation runs.

Nomenclature

A	flow area, m^2
A	aging activation energy, 1/s
API	API gravity, °API
b	sum of cleaning binary variables for all cleaning methods, dimensionless
b_k	cleaning binary variable for method k, dimensionless
c	mass concentration, kg/m^3
C_f	friction factor, dimensionless
C_p	specific heat capacity, J/kg
CCl	chemical cleaning
D	diameter, m
dir	direction of flow
E_a	aging activation energy, J/mol
E_f	fouling activation energy, J/mol
F/A	shell total force per unit area, N/m^2
h	heat transfer coefficient, W/m^2 K
H	specific enthalpy, J/kg
K_s	shell fouling-to-total fouling ratio, dimensionless
L	tube length, m
Lbb	bundle-to-baffle diametral clearance, m
Lsb	shell-to-baffle diametral clearance, m
Ltb	tube-to-baffle diametral clearance, m
Ltt	space between adjacent tubes, m
$\dot{m}$	mass flowrate, kg/s
MCl	mechanical cleaning
MeABP	mean average boiling point, °C
$n_{Cl,k}$	cleaning rate of method k, kg/m^2 s
$n_{f,i}$	fouling rate of component i, kg/m^2 s
NC	number of components
NCl	number of cleaning methods
NR	number of reactions
N_p	number of tube passes
N_s	number of shells
N_t	number of tubes
p	perimeter, m
P	pressure, Pa
P1, P2, P3	periods 1, 2, 3
Pr	Prandtl number, $C_p\mu/\lambda$, dimensionless
pt	pitch, m
Q	heat duty, W
q“	heat flux, W/m^2
R	radius, m
R_f	fouling resistance referred to outer tube area, m^2K/W
R_{flow}	radius at the fouling layer-fluid interface, m
R_g	ideal gas constant, 8.314 J/molK
r	radial coordinate, m
$\tilde{r}$	dimensionless radial coordinate
r_j	rate of reaction j, kg/m^3s
Re	Reynolds number, dimensionless
t	time, s
T	temperature, K
T_{film}	film temperature, K
u	linear velocity, m/s
z	axial coordinate, m

Greek symbols

α'	modified deposition constant, kg/m^2 s
γ'	modified removal constant, kg/m^2 s Pa
δ	deposit thickness, m
$\dot{\delta}$	rate of change in fouling layer thickness, m/s
ΔP	pressure drop, Pa
λ	thermal conductivity, W/mK
μ	dynamic viscosity, Pa s
ρ	density, kg/m^2
νij	stoichiometric coefficient for component i in reaction j
$\nu 38°C$	kinematic viscosity at 38°C, mm^2/s
τ	tube shear stress/shell total force per unit area, N/m^2
Ω	spatial domain

Subscripts

a	apparent
av	average
c	clean
Cl	cleaning
f	fouling
i	inner tube surface; component number
in	inlet
j	reaction number
k	cleaning method
l	layer
n	pass number
o	outer
out	outlet
s	shell
t	tube
w	wall

Superscripts

sim simulated

Notes on contributors

Emilio Diaz-Bejarano is a consultant at Hexxcell Ltd., where he works on the development of Hexxcell Studio™ and consulting services to oil and gas and process industries. He holds a degree in Chemical Engineering from Universidad de Salamanca, Spain, an M.Sc. and a Ph.D. in Chemical Engineering, both from Imperial College London. He was awarded an Iberdrola Foundation Scholarship for Master's Studies in Energy and the Environment and he was a recipient of the Geoff Hewitt Prize from Imperial College as the top student in the 2011 M.Sc. His research interests are in process systems engineering with focus on the development of mathematical models for heat exchange and energy systems.

Francesco Coletti is the Chief Technology Officer of Hexxcell Ltd. where he leads the development of Hexxcell Studio™ and the energy efficiency consulting practice serving blue chip companies. Prior to Hexxcell, he worked as a Development Specialist in the Cryogenic Systems R&D group at Praxair Inc., a Fortune 250 company in Buffalo, NY. He is the Executive Editor of *Heat Exchanger Design Handbook* and co-edited a monograph dedicated to crude oil fouling. He is also the Secretary of the UK National Heat Transfer Committee and an elected member of the Assembly for International Heat Transfer Conferences. He holds a Laurea degree in Chemical Engineering from the University of Padova, Italy, an M.Sc. in Process Systems Engineering and a Ph.D. in Chemical Engineering from Imperial College London.

Sandro Macchietto is a Professor of Process Systems Engineering in the Department of Chemical Engineering at Imperial College London. His research is on general methods for process systems engineering (simulation, optimization, and design of experiments) and their applications to process and energy systems. At Imperial, he co-founded the Centre for Process Systems Engineering, the Energy Futures Lab and launched the M.Sc. in Sustainable Energy Futures. He also launched two spinoff companies. He is a recipient of the 2007 McRobert Award, the top award for profitable innovation of the UK Royal Academy of Engineering and was made a Cavaliere of the Order of Merit by the Italian President in 2003.

ORCID

Emilio Diaz-Bejarano http://orcid.org/0000-0002-6387-2995
Francesco Coletti http://orcid.org/0000-0001-9445-0077
Sandro Macchietto http://orcid.org/0000-0001-6096-8126

References

[1] S. Macchietto et al., "Fouling in crude oil preheat trains: a systematic solution to an old problem," *Heat Transf. Eng.*, vol. 32, no. 3–4, pp. 197–215, Mar. 2011. DOI: 10.1080/01457632.2010.495579.

[2] F. Coletti and G. F. Hewitt, *Crude Oil Fouling: Deposit Characterization, Measurements, and Modeling*. Boston, MA, USA: Gulf Professional Publishing, 2014.

[3] S. Macchietto, "Energy efficient heat exchange in fouling conditions: the UNIHEAT Project," presented at the *Int. Conf. Heat Exchanger Fouling and Cleaning – 2015*, Enfield (Dublin), Ireland, Jun. 7–12, 2015.

[4] E. F. C. Somerscales, "Fouling of heat transfer surfaces an historical review," *Heat Transf. Eng.*, vol. 11, no. 1, pp. 19–36, 1990. DOI: 10.1080/01457639008939720.

[5] J. M. Chenoweth, "The TEMA Standards fouling section: another look," in *Fouling Mitigation of Industrial Heat-Exchange Equipment*, C. B. Panchal, Ed. New York, NY, USA: Begell House Inc., 1997.

[6] B. D. Crittenden, S. T. Kolaczkowski, and S. A. Hout, "Modelling hydrocarbon fouling," *Chem. Eng. Res. Des.*, vol. 65, no. 2, pp. 171–179, 1987.

[7] N. Epstein, "A model for the initial chemical reaction fouling rate for flow within a heated tube, and its verification," in *10th Int. Heat Transfer Conf.*, Vol. 4, I.Chem.E., Brighton, UK, August 14–18, 1994, pp. 225–229.

[8] G. T. Polley, D. I. Wilson, B. L. Yeap, and S. J. Pugh, "Evaluation of laboratory crude oil threshold fouling data for application to refinery pre-heat trains," *Appl. Therm. Eng.*, vol. 22, no. 7, pp. 777–788, May 2002. DOI: 10.1016/S1359-4311(02)00023-6.

[9] M. R. J. Nasr and M. M. Givi, "Modeling of crude oil fouling in preheat exchangers of refinery distillation units," *Appl. Therm. Eng.*, vol. 26, no. 14–15, pp. 1572–1577, Oct. 2006. DOI: 10.1016/j.applthermaleng.2005.12.001.

[10] B. L. Yeap, D. I. Wilson, G. T. Polley, and S. J. Pugh, "Mitigation of crude oil refinery heat exchanger fouling through retrofits based on thermo-hydraulic fouling models," *Chem. Eng. Res. Des.*, vol. 82, no. 1, pp. 53–71, 2004. DOI: 10.1205/026387604772803070.

[11] E. M. Ishiyama, F. Coletti, S. Macchietto, W. R. Paterson, and D. I. Wilson, "Impact of deposit ageing on thermal fouling: lumped parameter model," *AIChE J.*, vol. 56, no. 2, pp. 531–545, 2010.

[12] F. Coletti, E. M. Ishiyama, W. R. Paterson, D. I. Wilson, and S. Macchietto, Impact of deposit aging and surface roughness on thermal fouling: distributed model," *AIChE J.*, vol. 56, no. 12, pp. 3257–3273, 2010. DOI: 10.1002/aic.12221.

[13] M. C. Georgiadis, G. E. Rotstein, and S. Macchietto, "Modeling and simulation of shell and tube heat exchangers under milk fouling," *AIChE J.*, vol. 44, no. 4, pp. 959–971, 1998. DOI: 10.1002/aic.690440422.

[14] T. Tinker, "Shell–side characteristics of shell–and–tube heat exchangers," *Trans. ASME*, vol. 80, no. 1, pp. 36–52, 1958.

[15] K. J. Bell, "Final report of the cooperative research program on shell and tube heat exchangers," in *University of Delaware Engineering Experimental Station Bulletin No. 5*, Newark, DE, USA: University of Delaware, Engineering Experimental Station, 1963.

[16] J. Taborek, "Calculation of heat transfer coefficient and pressure drop," in *Heat Exchanger Design Handbook*, G. F. Hewitt, Ed. Redding, NC, USA: Begell House, 2008.

[17] G. F. Hewitt, "Flow stream analysis method for segmentally baffled shell and tube heat exchangers," in *Heat Exchanger Design Handbook*, G. F. Hewitt, Ed. Redding, NC, USA: Begell House, 2008.

[18] R. H. Clarke and F. Nicolas, "CFD Investigation of maldistribution effects on crude-oil fouling in shell and tube exchangers," in *Second International Conference on Petroleum and Gas Phase Behaviour and Fouling*, Copenhagen, Denmark, Aug. 27–31, 2000.

[19] W. A. Ebert and C. B. Panchal, "Analysis of exxon crude-oil slip stream coking data," in *Fouling Mitigation of Industrial Heat-Exchange Equipment*, San Luis Obispo, CA, USA, June 18–23, 1995, pp. 451–460.

[20] P. Vessakosol and J. Charoensuk, "Numerical analysis of heat transfer and flow field around cross-flow heat exchanger tube with fouling," *Appl. Therm. Eng.*, vol. 30, no. 10, pp. 1170–1178, Jul. 2010. DOI: 10.1016/j.applthermaleng.2010.01.034.

[21] A. Zbogar, F. Frandsen, P. A. Jensen, and P. Glarborg, "Shedding of ash deposits," *Prog. Energy Combust. Sci.*, vol. 35, no. 1, pp. 31–56, 2009. DOI: 10.1016/j.pecs.2008.07.001.

[22] M. Garcia Perez, E. Vakkilainen, and T. Hyppanen, The contribution of differently-sized ash particles to the fouling trends of a pilot-scale coal-fired combustor with an ash deposition CFD model," *Fuel*, vol. 189 (1 February), pp. 120–130, 2017. DOI: 10.1016/j.fuel.2016.10.090.

[23] E. Diaz-Bejarano and F. Coletti, "Modelling of shell-side crude oil fouling in shell-and-tube heat exchangers," in *Int. Conf. Heat Exchanger Fouling and Cleaning – 2015*, Enfield (Dublin), Ireland, Jun. 7–12, 2015, pp. 81–88.

[24] F. Coletti and S. Macchietto, "A dynamic, distributed model of shell-and-tube heat exchangers undergoing crude oil fouling," *Ind. Eng. Chem. Res.*, vol. 50, no. 8, pp. 4515–4533, Apr. 2011. DOI: 10.1021/ie901991g.

[25] R. K. Sinnot, *Coulson and Richardson's Chemical Engineering; Volume 6, Chemical Engineering Design*, 3rd ed. Oxford, UK: Butterworth Heinemann, 1999.

[26] J. Henry, "Headers, nozzles, and turnarounds," in *Heat Exchanger Design Handbook*, G. F. Hewitt, Ed. Redding, NC, USA: Begell House, 2008.

[27] E. A. D. Saunders, *Heat exchangers: Selection, Design, and Construction*. Harlow, UK: Longman, 1988.

[28] J. P. Holman, *Heat transfer*, 8th ed. London, UK: McGraw-Hill, 2001.

[29] J. Taborek, "Shell-and-tube heat exchangers: single phase flow," in *Heat Exchanger Design Handbook*, G. F. Hewitt, Ed. New York, NY, USA: Begell House, 2002.

[30] E. Diaz-Bejarano, E. Behranvand, F. Coletti, M. R. Mozdianfard, and S. Macchietto, "Organic and inorganic fouling in heat exchangers – industrial case study: analysis of fouling state, *Appl. Energy*, vol. 206, pp. 1250–1266, 2017. doi:10.1016/j.apenergy.2017.10.018.

[31] E. Diaz-Bejarano, F. Coletti, and S. Macchietto, "A new dynamic model of crude oil fouling deposits and its application to the simulation of fouling-cleaning cycles," *AIChE J.*, vol. 62, no. 1, pp. 90–107, 2016. doi:10.1002/aic.15036.

[32] A. Zukauskas, and R. Ulinskas, "Banks of plain and finned tubes," in *Heat Exchanger Design Handbook*, G. F. Hewitt, Ed. Redding, NC, USA: Begell House, 2008.

[33] Hexxcell Ltd., "Hexxcell studio," 2018. [Online]. Available: http://www.hexxcell.com. (Accessed February 28, 2018)

[34] E. Diaz-Bejarano, F. Coletti, and S. Macchietto, "Thermohydraulic analysis of refinery heat exchangers undergoing fouling," *AIChE J.*, vol. 63, no. 3, pp. 984–1001, 2017. DOI: 10.1002/aic.15457.

[35] L. Lanchas-Fuentes, E. Diaz-Bejarano, F. Coletti, and S. Macchietto, "Management of cleaning types and schedules in refinery heat exchangers," in *12th International Conference on Heat Transfer, Fluid Mechanics and Thermodynamics*, Malaga, Spain, July 11–13, 2016.

[36] Process Systems Enterprise, gPROMS. Process Systems Enterprise Ltd., 2018.

[37] M. R. Riazi, *Characterization and Properties of Petroleum Fractions*, 1st ed. Philadelphia, PY, USA: ASTM, 2005.

[38] A. P. Watkinson, *Critical Review of Organic Fluid Fouling*. Argonne, IL, USA, 1988.

[39] E. Diaz-Bejarano, F. Coletti, and S. Macchietto, "Impact of complex layering structures of organic and inorganic foulants on the thermohydraulic performance of a single heat exchanger tube: a simulation study," *Ind. Eng. Chem. Res.*, vol. 55, no. 40, pp. 10718–10734, 2016. DOI: 10.1021/acs.iecr.6b02330.

[40] C. B. Panchal, W. C. Kuru, C. F. Liao, W. A. Ebert, and J. W. Palen, "Threshold conditions for crude oil fouling," in *Understanding Heat Exchanger Fouling and Its Mitigation*, Castelvecchio Pascoli, Italy, May 11–16, 1997. New York, NY, USA: Begell House, 1999, pp. 273–279.

[41] E. Diaz-Bejarano, M. Yugo Santos, M. Garcia Dopico, L. Lanchas-Fuentes, and F. Coletti, "The impact of fouling on the optimal design of a heat exchanger network: an industrial case study," in *Heat Exchanger Fouling and Cleaning – 2017*, Aranjuez (Madrid), Spain, pp. 11–16, June 2017.